SINTEF
PROCEEDINGS
2

Proceedings of the 12th International Conference on Computational Fluid Dynamics in the Oil & Gas, Metallurgical and Process Industries

# Progress in Applied CFD – CFD2017

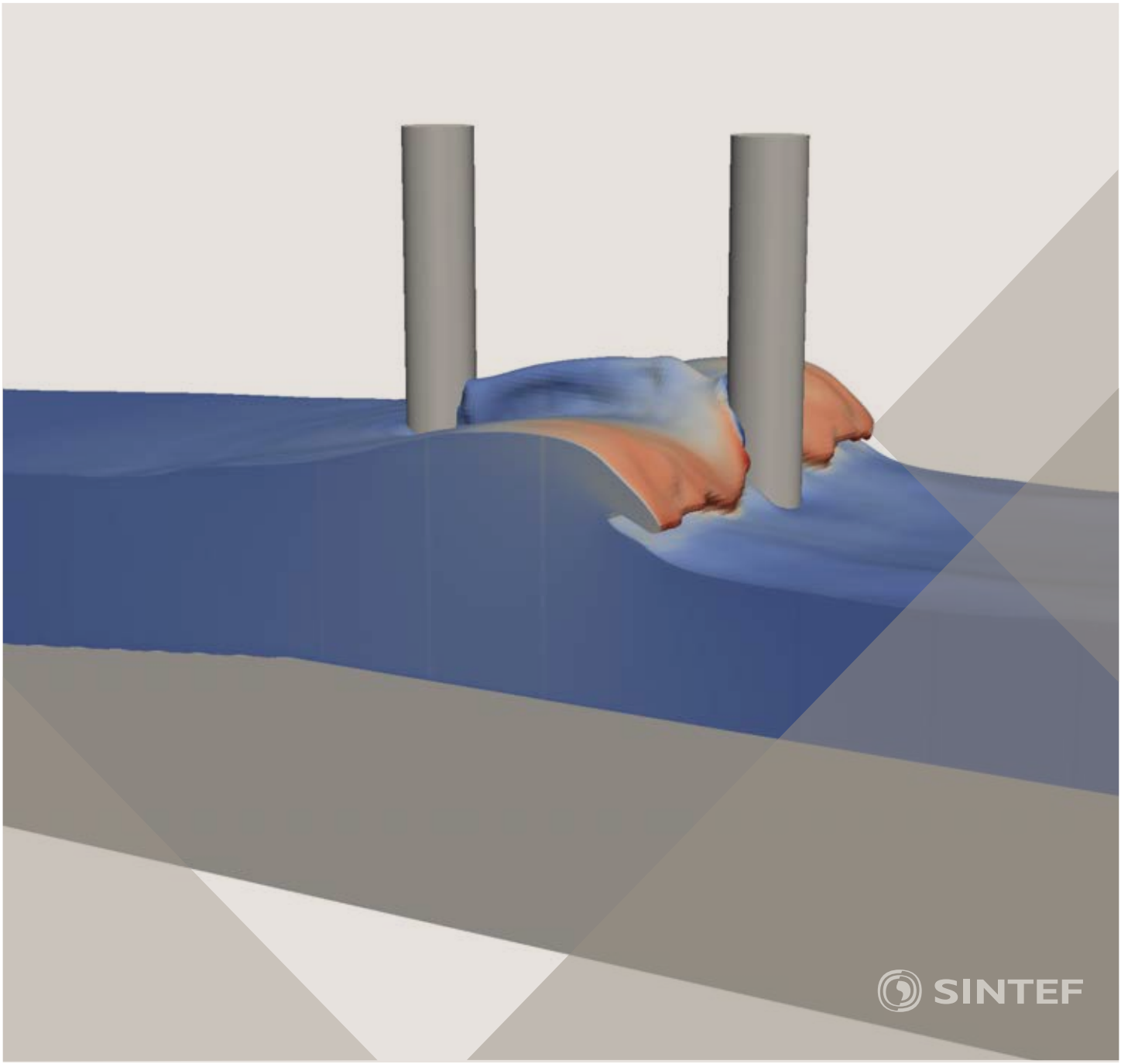

SINTEF Proceedings

Editors:
Jan Erik Olsen and Stein Tore Johansen

# Progress in Applied CFD – CFD2017

Proceedings of the 12th International Conference on Computational Fluid Dynamics in the Oil & Gas, Metallurgical and Process Industries

SINTEF Academic Press

SINTEF Proceedings no 2
Editors: Jan Erik Olsen and Stein Tore Johansen
**Progress in Applied CFD – CFD2017**
Selected papers from 10th International Conference on Computational Fluid Dynamics in the Oil & Gas, Metallurgical and Process Industries

Key words:
CFD, Flow, Modelling

Cover, illustration: Arun Kamath

ISSN 2387-4295 (online)
ISBN 978-82-536-1544-8 (pdf)



SINTEF Academic Press
Address: Forskningsveien 3 B
PO Box 124 Blindern
N-0314 OSLO
Tel: +47 73 59 30 00
Fax: +47 22 96 55 08

www.sintef.no/byggforsk
www.sintefbok.no

**SINTEF Proceedings**
SINTEF Proceedings is a serial publication for peer-reviewed conference proceedings on a variety of scientific topics.
The processes of peer-reviewing of papers published in SINTEF Proceedings are administered by the conference organizers and proceedings editors. Detailed procedures will vary according to custom and practice in each scientific community.

## PREFACE

This book contains all manuscripts approved by the reviewers and the organizing committee of the 12th International Conference on Computational Fluid Dynamics in the Oil & Gas, Metallurgical and Process Industries. The conference was hosted by SINTEF in Trondheim in May/June 2017 and is also known as CFD2017 for short. The conference series was initiated by CSIRO and Phil Schwarz in 1997. So far the conference has been alternating between CSIRO in Melbourne and SINTEF in Trondheim. The conferences focuses on the application of CFD in the oil and gas industries, metal production, mineral processing, power generation, chemicals and other process industries. In addition pragmatic modelling concepts and bio-mechanical applications have become an important part of the conference. The papers in this book demonstrate the current progress in applied CFD.

The conference papers undergo a review process involving two experts. Only papers accepted by the reviewers are included in the proceedings. 108 contributions were presented at the conference together with six keynote presentations. A majority of these contributions are presented by their manuscript in this collection (a few were granted to present without an accompanying manuscript).

The organizing committee would like to thank everyone who has helped with review of manuscripts, all those who helped to promote the conference and all authors who have submitted scientific contributions. We are also grateful for the support from the conference sponsors: ANSYS, SFI Metal Production and NanoSim.

Stein Tore Johansen & Jan Erik Olsen



Organizing committee:

Conference chairman: Prof. Stein Tore Johansen
Conference coordinator: Dr. Jan Erik Olsen
Dr. Bernhard Müller
Dr.Sigrid Karstad Dahl
Dr.Shahriar Amini
Dr.Ernst Meese
Dr.Josip Zoric
Dr.Jannike Solsvik
Dr.Peter Witt

Scientific committee:

Stein Tore Johansen, SINTEF/NTNU
Bernhard Müller, NTNU
Phil Schwarz, CSIRO
Akio Tomiyama, Kobe University
Hans Kuipers, Eindhoven University of Technology
Jinghai Li, Chinese Academy of Science
Markus Braun, Ansys
Simon Lo, CD-adapco
Patrick Segers, Universiteit Gent
Jiyuan Tu, RMIT
Jos Derksen, University of Aberdeen
Dmitry Eskin, Schlumberger-Doll Research
Pär Jönsson, KTH
Stefan Pirker, Johannes Kepler University
Josip Zoric, SINTEF

## CONTENTS

**PRAGMATIC MODELLING ..... 9**
On pragmatism in industrial modeling. Part III: Application to operational drilling ..... 11
CFD modeling of dynamic emulsion stability ..... 23
Modelling of interaction between turbines and terrain wakes using pragmatic approach ..... 29

**FLUIDIZED BED ..... 37**
Simulation of chemical looping combustion process in a double looping fluidized bed reactor with cu-based oxygen carriers ..... 39
Extremely fast simulations of heat transfer in fluidized beds ..... 47
Mass transfer phenomena in fluidized beds with horizontally immersed membranes ..... 53
A Two-Fluid model study of hydrogen production via water gas shift in fluidized bed membrane reactors ..... 63
Effect of lift force on dense gas-fluidized beds of non-spherical particles ..... 71
Experimental and numerical investigation of a bubbling dense gas-solid fluidized bed ..... 81
Direct numerical simulation of the effective drag in gas-liquid-solid systems ..... 89
A Lagrangian-Eulerian hybrid model for the simulation of direct reduction of iron ore in fluidized beds ..... 97
High temperature fluidization - influence of inter-particle forces on fluidization behavior ..... 107
Verification of filtered two fluid models for reactive gas-solid flows ..... 115

**BIOMECHANICS ..... 123**
A computational framework involving CFD and data mining tools for analyzing disease in cartoid artery ..... 125
Investigating the numerical parameter space for a stenosed patient-specific internal carotid artery model ..... 133
Velocity profiles in a 2D model of the left ventricular outflow tract, pathological case study using PIV and CFD modeling ..... 139
Oscillatory flow and mass transport in a coronary artery ..... 147
Patient specific numerical simulation of flow in the human upper airways for assessing the effect of nasal surgery ..... 153
CFD simulations of turbulent flow in the human upper airways ..... 163

**OIL & GAS APPLICATIONS ..... 169**
Estimation of flow rates and parameters in two-phase stratified and slug flow by an ensemble Kalman filter ..... 171
Direct numerical simulation of proppant transport in a narrow channel for hydraulic fracturing application ..... 179
Multiphase direct numerical simulations (DNS) of oil-water flows through homogeneous porous rocks ..... 185
CFD erosion modelling of blind tees ..... 191
Shape factors inclusion in a one-dimensional, transient two-fluid model for stratified and slug flow simulations in pipes ..... 201
Gas-liquid two-phase flow behavior in terrain-inclined pipelines for wet natural gas transportation ..... 207

**NUMERICS, METHODS & CODE DEVELOPMENT ..... 213**
Innovative computing for industrially-relevant multiphase flows ..... 215
Development of GPU parallel multiphase flow solver for turbulent slurry flows in cyclone ..... 223
Immersed boundary method for the compressible Navier–Stokes equations using high order summation-by-parts difference operators ..... 233
Direct numerical simulation of coupled heat and mass transfer in fluid-solid systems ..... 243
A simulation concept for generic simulation of multi-material flow, using staggered Cartesian grids ..... 253
A cartesian cut-cell method, based on formal volume averaging of mass, momentum equations ..... 265
SOFT: a framework for semantic interoperability of scientific software ..... 273

**POPULATION BALANCE ..... 279**
Combined multifluid-population balance method for polydisperse multiphase flows ..... 281
A multifluid-PBE model for a slurry bubble column with bubble size dependent velocity, weight fractions and temperature ..... 285
CFD simulation of the droplet size distribution of liquid-liquid emulsions in stirred tank reactors ..... 295
Towards a CFD model for boiling flows: validation of QMOM predictions with TOPFLOW experiments ..... 301
Numerical simulations of turbulent liquid-liquid dispersions with quadrature-based moment methods ..... 309
Simulation of dispersion of immiscible fluids in a turbulent couette flow ..... 317
Simulation of gas-liquid flows in separators - a Lagrangian approach ..... 325
CFD modelling to predict mass transfer in pulsed sieve plate extraction columns ..... 335

**BREAKUP & COALESCENCE ..... 343**
Experimental and numerical study on single droplet breakage in turbulent flow ..... 345
Improved collision modelling for liquid metal droplets in a copper slag cleaning process ..... 355
Modelling of bubble dynamics in slag during its hot stage engineering ..... 365
Controlled coalescence with local front reconstruction method ..... 373

**BUBBLY FLOWS ..... 381**
Modelling of fluid dynamics, mass transfer and chemical reaction in bubbly flows ..... 383
Stochastic DSMC model for large scale dense bubbly flows ..... 391
On the surfacing mechanism of bubble plumes from subsea gas release ..... 399
Bubble generated turbulence in two fluid simulation of bubbly flow ..... 405

**HEAT TRANSFER ..... 413**
CFD-simulation of boiling in a heated pipe including flow pattern transitions using a multi-field concept ..... 415
The pear-shaped fate of an ice melting front ..... 423
Flow dynamics studies for flexible operation of continuous casters (flow flex cc) ..... 431
An Euler-Euler model for gas-liquid flows in a coil wound heat exchanger ..... 441

**NON-NEWTONIAN FLOWS ..... 449**
Viscoelastic flow simulations in disordered porous media ..... 451
Tire rubber extrudate swell simulation and verification with experiments ..... 459
Front-tracking simulations of bubbles rising in non-Newtonian fluids ..... 469
A 2D sediment bed morphodynamics model for turbulent, non-Newtonian, particle-loaded flows ..... 479

**METALLURGICAL APPLICATIONS ..... 491**
Experimental modelling of metallurgical processes ..... 493
State of the art: macroscopic modelling approaches for the description of multiphysics phenomena within the electroslag remelting process ..... 499
LES-VOF simulation of turbulent interfacial flow in the continuous casting mold ..... 507
CFD-DEM modelling of blast furnace tapping ..... 515
Multiphase flow modelling of furnace tapholes ..... 521
Numerical predictions of the shape and size of the raceway zone in a blast furnace ..... 531
Modelling and measurements in the aluminium industry - Where are the obstacles? ..... 541
Modelling of chemical reactions in metallurgical processes ..... 549
Using CFD analysis to optimise top submerged lance furnace geometries ..... 555
Numerical analysis of the temperature distribution in a martensic stainless steel strip during hardening ..... 565
Validation of a rapid slag viscosity measurement by CFD ..... 575
Solidification modeling with user defined function in ANSYS Fluent ..... 583
Cleaning of polycyclic aromatic hydrocarbons (PAH) obtained from ferroalloys plant ..... 587
Granular flow described by fictitious fluids: a suitable methodology for process simulations ..... 593
A multiscale numerical approach of the dripping slag in the coke bed zone of a pilot scale Si-Mn furnace ..... 599

**INDUSTRIAL APPLICATIONS ..... 605**
Use of CFD as a design tool for a phospheric acid plant cooling pond ..... 607
Numerical evaluation of co-firing solid recovered fuel with petroleum coke in a cement rotary kiln: Influence of fuel moisture ..... 613
Experimental and CFD investigation of fractal distributor on a novel plate and frame ion-exchanger ..... 621

**COMBUSTION ..... 631**
CFD modeling of a commercial-size circle-draft biomass gasifier ..... 633
Numerical study of coal particle gasification up to Reynolds numbers of 1000 ..... 641
Modelling combustion of pulverized coal and alternative carbon materials in the blast furnace raceway ..... 647
Combustion chamber scaling for energy recovery from furnace process gas: waste to value ..... 657

**PACKED BED ..... 665**
Comparison of particle-resolved direct numerical simulation and 1D modelling of catalytic reactions in a packed bed ..... 667
Numerical investigation of particle types influence on packed bed adsorber behaviour ..... 675
CFD based study of dense medium drum separation processes ..... 683
A multi-domain 1D particle-reactor model for packed bed reactor applications ..... 689

**SPECIES TRANSPORT & INTERFACES ..... 699**
Modelling and numerical simulation of surface active species transport - reaction in welding processes ..... 701
Multiscale approach to fully resolved boundary layers using adaptive grids ..... 709
Implementation, demonstration and validation of a user-defined wall function for direct precipitation fouling in Ansys Fluent ..... 717

**FREE SURFACE FLOW & WAVES ..... 727**
Unresolved CFD-DEM in environmental engineering: submarine slope stability and other applications ..... 729
Influence of the upstream cylinder and wave breaking point on the breaking wave forces on the downstream cylinder ..... 735
Recent developments for the computation of the necessary submergence of pump intakes with free surfaces ..... 743
Parallel multiphase flow software for solving the Navier-Stokes equations ..... 752

**PARTICLE METHODS ..... 759**
A numerical approach to model aggregate restructuring in shear flow using DEM in Lattice-Boltzmann simulations ..... 761
Adaptive coarse-graining for large-scale DEM simulations ..... 773
Novel efficient hybrid-DEM collision integration scheme ..... 779
Implementing the kinetic theory of granular flows into the Lagrangian dense discrete phase model ..... 785
Importance of the different fluid forces on particle dispersion in fluid phase resonance mixers ..... 791
Large scale modelling of bubble formation and growth in a supersaturated liquid ..... 798

**FUNDAMENTAL FLUID DYNAMICS ..... 807**
Flow past a yawed cylinder of finite length using a fictitious domain method ..... 809
A numerical evaluation of the effect of the electro-magnetic force on bubble flow in aluminium smelting process ..... 819
A DNS study of droplet spreading and penetration on a porous medium ..... 825
From linear to nonlinear: Transient growth in confined magnetohydrodynamic flows ..... 831

# FLOW DYNAMICS STUDIES FOR FLEXIBLE OPERATION OF CONTINUOUS CASTERS (FLOW FLEX CC)

**Tobias Forslund[1, 2], Henrik Barestrand[2], Pavel E. Ramirez Lopez[1], Pooria Jalali[1], Christer Olofsson[1] Tobias Lindbäck[1] and Erik Roos[3]**

[1] Process Metallurgy Department, Swerea MEFOS, Luleå, SWEDEN
[2] Luleå University of Technology (LTU), Luleå, SWEDEN
[3] SSAB Special Steels, Oxelösund, SWEDEN

* E-mail: tobias.forslund@swerea.se

## ABSTRACT

Flow dynamics of liquid steel within the Continuous Casting (CC) mould are critical for process stability and the quality of final products. An "optimal" flow provides enough circulation of the metal to avoid freezing, but it is stable enough to avoid defects during solidification. This requires a trade-off between speed and stability that is difficult to achieve for the variety of conditions faced by the Scandinavian steel industry (e.g. small orders with high variability in size and steel grades). This is difficult to address with typical CFD models used by the industry and suppliers for design of flow control devices (nozzle, stoppers, etc.), since flow optimization requires a better understanding of the level instabilities inside the mould (i.e. free surface) and its highly turbulent behaviour. Consequently, CC requires advanced multiphase models as well as accurate turbulent and time scales resolution.

The investigation presented uses a multiphase approach (Volume of Fluid, VOF + Discrete Phase Modelling, DPM) to solve the molten steel and argon injection within the mould combined with Large Eddy Simulation (LES) to improve the resolution of turbulent scales compared to typical 2-equation models. CFD simulations were successfully validated with results from a Continuous Casting Simulator using a low melting point alloy. Then, these tools were used to design and test different SEN types for various mould sizes in order to optimize their flow pattern and performance in the mould. The project included a comprehensive set of plant trials at an industrial caster to validate/calibrate model predictions, test nozzle resistance and explore process improvement opportunities.

**Keywords:** Numerical modelling, Continuous Casting, SEN, LES, design, optimization.

## NOMENCLATURE

$g$, Gravitational acceleration $[m/s^2]$

$\phi$, Velocity potential $[m^2/s]$

$\{d, a, b\}$, Spatial lengths $[m]$

$\{x, y, z\}$, Spatial coordinates $[m]$

$\eta$, Surface offset $[m]$

$f$, Frequency in Hz $[1/s]$

$F_d(d)$, Dimensionless scaling function

$\rho$, Density $[kg/m^3]$

$D$, Nozzle port diameter (mm)

$\theta$, Nozzle port angle (mm)

$V$, Velocity $[m/s]$

$\{m, n\}$, integer numbers

## INTRODUCTION

The Swedish steel industry currently operates in a niche market where orders are small and products can differ significantly in composition and size. Thus, steelmakers seek a deeper process understanding to enhance quality for short production runs. Common quality problems in CC are related to flow instabilities in the mould, which may cause slag entrapment and cracking due to differences in shrinking and solidification for the variety of slab sizes ordered by the customers. The movement of liquid steel within the mould is critical to process stability and quality of final products where an "appropriate" behaviour of the metal level ensures a minimum of defects during solidification (Dauby, 2011). Therefore, there is a demand for a more flexible production where stable casting conditions are reached promptly to minimize defects. Consequently, the metal flow in the mould has been widely studied through simplified numerical models and physical models with water. Unfortunately, these approaches are not enough to capture the behaviour of the interface between metal and slag (e.g. single phase models) as well as the magnitude and frequency of level fluctuations at the interface due to different physical properties of liquid metal and water (e.g. water models). Advanced multiphase models are an efficient tool to address these shortcomings as well as testing different mould and nozzle geometries in a cost and time efficient manner. The advanced simulations carried out in this investigation use LES (Large Eddy Simulation) coupled to a DPM (Discrete Phase Model) model developed by Olsen *et al.* (Olsen *et al.*, 2009) for stirred ladles. This has been adapted to handle Argon gas injection in the nozzle and flow dynamics in the Continuous Casting mould (Ramirez Lopez *et al.*, 2014).

## The Continuous Casting (CC) process

Continuous Casting is a process by which molten metal is poured from a ladle into a copper mould through a Submerged Entry Nozzle (SEN). The metal fills the mould and forms a solidifying shell which contains the liquid steel as it is slowly pulled out at a specified casting speed ($m/min$). Slag is added on top of the mould forming a slag-metal interface which prevents direct contact with air to avoid re-oxidation. As the strand is drawn out, it is bent by a series of cylindrical rolls. Once the strand has completely solidified it is cut into slabs by a gas torch. Figure 1 presents an overview of the CC process where red represents liquid metal, blue illustrates the solidified shell in the strand and grey represents the slag cover.

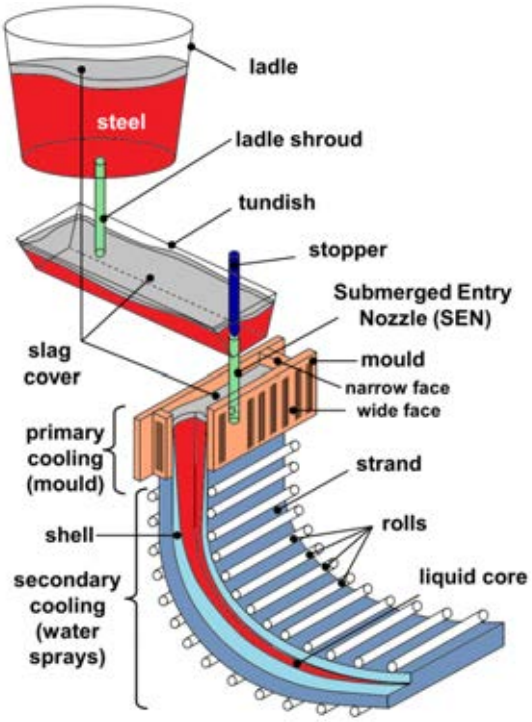


**Figure 1:** CC-Mould process.

## Numerical modelling

There are several complex physical processes acting simultaneously in the mould during casting. Firstly, there is a strong recirculating flow of liquid steel which is determined by the nozzle shape and mould size. Secondly, the injection of Argon (small bubbles, typically <5 mm in ∅) affects the main flow and disturbs the metal level as they leave the surface. Additionally, the slag acts as a semi-wall by dampening the fluctuations at the slag-metal interface (Pericleous *et al.*, 2010). This behaviour is highly dependent on the SEN design, mould and casting conditions. Furthermore, in some cases, external fields such as electro-magnetic breaking and/or stirring can be used to modify the flow. However, a model able to capture each of these phenomena to the smallest detail is not feasible for industrial application. Therefore, several simplifications have to be made in order to achieve predictions with enough accuracy at a reasonable computational cost. These include the following:

- Viscosity and density variations with temperature do not affect to a large extent the flow in the mould. Thus, the flow is assumed to be isothermal.
- The mushy zone close to the solidified shell in the mould walls can be approximated by a non-slip wall.
- The hydrostatic pressure and temperature variations in the liquid steel do not affect the Argon bubbles diameter significantly.
- The mesh is adapted for computational efficiency. Thus, boundary layers are not fully resolved at the walls (e.g. not ensuring $y^+ \approx 1$) while time-step increments do not achieve Courant numbers below 1 in all of the geometry. However, it was concluded that an element count of ~2 Million cells provides a good compromise between accuracy and computational time for the available resources. A mesh study has been carried out to verify the accuracy of the simulations (Barestrand *et al.*, 2016).

Figure 2 illustrates the geometry and different mesh zones for the model, (1) is a constant velocity inlet, (2) is a pressure outlet and (3) is a constant velocity outlet.

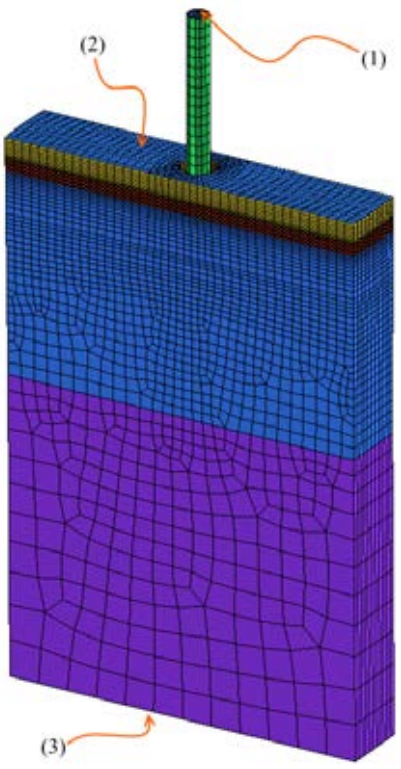


**Figure 2:** Mould model geometry & coarse mesh.

The mesh is completely conformal and joined by transition zones. It is highly refined at the metal level (red) and nozzle (green) to enable capturing of surface fluctuations and turbulence. The SIMPLE C-algorithm is used together with a Least Squares Cell Based gradient description for time-stepping. A body force weighted formulation was used for pressure, whereas a bounded central differencing is used for momentum. A second order upwind scheme is used for the volume fraction.

The following parameters were used for the LES (turbulence), VOF (Eulerian frame) and DPM (Lagrangian frame) sub-models for solving the Navier-Stokes equations:

- Large Eddy Simulation
  - WALE Subgrid model
  - WALE constant (Cw = 0.325)
- VOF: Eulerian frame type model
  - Implicit body force
  - Dispersed interface
  - Constant interfacial surface tension
- Discrete phase model:
  - Updated every third time-step
  - Coalescence
  - Custom User Defined Function (UDF) for drag-force
- Two-way coupling interaction between continuous phase (steel) and Disperse phase (Argon bubbles) including turbulent interactions.

Further details on the standard solver are not discussed here in detail since they can be found in the ANSYS-FLUENT theory manual (ANSYS-Inc., 2013) while specific changes to the solution procedure and User Defined Functions can be found in a detailed report (Barestrand *et al.*, 2016). ANSYS-FLUENT was executed on a 128 core cluster.

## Physical modelling

A numerical model that aims to incorporate all the phenomena described previously needs substantial amounts of data for validation. This was partly done at a Continuous Casting simulator located at Swerea MEFOS. The simulator is based on a low-melting point alloy with similar properties to liquid steel. The properties used in the CFD simulations for steel and the low melting point alloy in the casting simulator is presented on Table 1.

**Table 1:** Casting Simulator Details and material properties

| **Continuous Casting Simulator specifications** | | | |
|---|---|---|---|
| Mould size | 1.2 x 0.22 x 0.9 m | | |
| Tundish (metal holder) | h = 0.7-0.9 m | | |
| Argon flow rate | Variable : up to 12 lit/min | | |
| Immersion depth | Variable within 150 mm | | |
| **Bi-Sn alloy (MCP-137) & liquid steel properties** | | | |
| | viscosity, $\mu$ (Pa-s x$10^{-3}$) | density, $\rho$ (kg/$m^3$) | kinematic viscosity, $\nu$ ($m^2$/s x$10^{-6}$) |
| Steel (1500 C°) | 6.28 | 7193.7 | 0.9 |
| MCP 137 (150 C°) | 10.7 | 8580 | 1.25 |
| MCP 137 (170 C°) | 8.6 | 8580 | 1 |

Further details on the CC simulator were presented previously at CFD 2014 in Trondheim (Ramirez Lopez *et al.*, 2014) (Figure 3).

**Figure 3:** CCS-1.5 Continuous Casting SimulatorThe CC simulator was used to test two different SEN types; namely mountain and cup, based on the shape of the bottom of the nozzle and ports (Figure 4). The mountain and cup types are designated M and C, respectively.

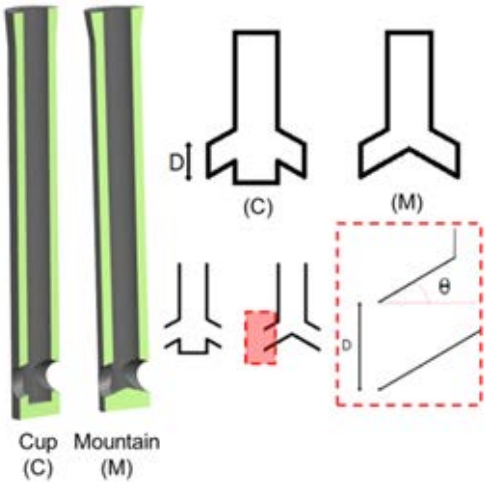


**Figure 4:** Mountain & Cup nozzle geometries and design parameters.

Experiments were carried out for all the casting conditions in the operational range of the industrial caster under investigation as well as testing the resistance and performance of the new nozzle designs. The industrial mould size varied between 1200 mm to 1680 mm in width and 220 mm to 290 mm in thickness, whereas validation in the CC simulator was carried out in a mould with 1200 mm width and 220 mm thickness for both nozzles. An optical probe was used for characterization of the surface fluctuations by means of a distance measurement with high acquisition rate, which resulted in reliable evaluation of the surface behaviour for the different nozzles and casting conditions (Figure 5a). The signal accuracy of the probe is up to 0.4 $\mu m$ with a sampling frequency of 1000 $Hz$. The probe was positioned at half the distance between the mould short face and nozzle as well as in the middle of the thickness for all measurements (Figure 5b-5c).

Large transient events were discarded in the processing of these signals, which leaves only the short period variations (e.g. *Ts<5s)* to characterize the fluctuations at the metal interface.

**Figure 5:** Measurement of fluctuations at the metal interface using an optical probe.

## Plant trials

A variety of velocity and surface profile measurements were carried out during actual production runs at an industrial CC machine. The velocity measurements were done using the nail board method where a rack of nails is dipped for a few seconds in the mould between the nozzle and narrow side. The steel forms a solidified tip whose profile can be related to the velocity and direction of the steel flow at that moment (Figure 6) (Liu *et al.*, 2011).

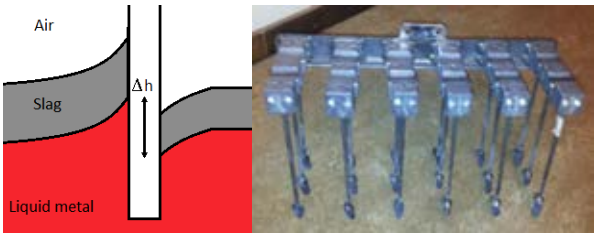


**Figure 6:** Schematics of nail dipped into the molten steel-slag interface (left) and nail board rack (right).

The velocity of the liquid metal at the nail position may be approximated by the formula.

$$\Delta h = \frac{V^2}{2g} \tag{1}$$

Where $\Delta h$ is the difference in height between the two sides of the nail; $V$ is the velocity at the interface and $g$ is the gravitational acceleration. The nail board presented in Figure 6 (right) provides a 3x6 resolution map of the interface velocities. Furthermore, the main flow direction may be determined by measuring the positions of maximum and minimum height of solidified tip on the nail. These measurements were used as basis to validate the velocities and level fluctuations measured in the Casting Simulator and CFD models.

## Analytical model

The analytical behaviour of surface waves has been extensively studied for liquids with a free surface (Lighthill, 2001). Thus, the free surface frequencies of the metal in the mould can be derived by assuming two completely inviscid fluids with density ($\rho$ and $\rho_x$) separated by an interface ($z = 0$) confined into a rectangular geometry of $Size_i = \{a, b, d\}$. The velocity potential in the fluids may be regarded as a general function dependent on spatial position and time. Further, it may be also assumed to be separable; so, the velocity potential can be written as:

$$\phi = \phi(x_j, t) = \phi_x(x)\phi_y(y)\phi_z(z)\phi_t(t) \tag{2}$$

Naturally, the velocity potential needs to satisfy the continuity equation since an incompressible fluid is assumed. Thus, this can be written as:

$$\frac{\partial^2 \phi}{\partial x_i \partial x_i} = 0 \tag{3}$$

If a new variable $\eta$ is introduced to represent the offset of the surface from position $z = 0$, the boundary conditions for the domain can be written as:

$$\left.\frac{\partial \phi}{\partial z}\right|_{z=-d} = 0;\ \left.\frac{\partial \phi}{\partial x}\right|_{x=0,a} = 0;\ \left.\frac{\partial \phi}{\partial z}\right|_{z=0} = \frac{\partial \eta}{\partial t};\ \left.\frac{\partial \phi}{\partial y}\right|_{y=0,b} = 0 \tag{4}$$

Where $a$ represents the width of the geometry containing the fluid, $b$ is the length and $d$ is the depth. The last condition for the interface comes from Bernoulli's equation for unsteady flows:

$$\frac{\partial \phi}{\partial t} + gz + \frac{p}{\rho} + \frac{1}{2}(\nabla \phi)^2 = 0 \tag{5}$$

Linearizing this equation (omitting $(\nabla \phi)^2$) gives the final boundary condition for Equation 6:

$$\left.\frac{\partial \phi}{\partial t}\right|_{z=0} + g\eta(x, y, t) + \frac{p}{\rho} = 0 \tag{6}$$

The derivation is straightforward by inserting Equation 2 into Equation 3. An oscillatory solution with the frequency (Equation 7) is obtained after applying the boundary conditions (Equations 4 and 6):

$$\begin{cases} f_{mn}^{\ 2} = \dfrac{g}{4\pi}\sqrt{\left(\dfrac{m}{a}\right)^2 + \left(\dfrac{n}{b}\right)^2}\, F_d(d) \\ F_d(d) = \tanh\left(\pi d^2 \sqrt{\left(\dfrac{m}{a}\right)^2 + \left(\dfrac{n}{b}\right)^2}\right), (m,n) \in \mathrm{Z}^+ \end{cases} \tag{7}$$

Where $a$ and $b$ are the side lengths (e.g. mould width and thickness) and $g$ is the gravitational acceleration. Note that this expression only holds true when there is significant density differences between the fluids (e.g. water and air). The frequencies obtained through this equation are the *eigenfrequencies* at which the liquid steel within the mould resonates. These frequencies are independent of viscosity, density and all other properties of the fluid (i.e. these are only a result of the interaction between continuity and body forces).
The general expression for the eigenfrequencies, ignoring the mould depth can be written as in Equation 8:

$$f_{mn}^{\ 2} = \frac{g}{4\pi}\sqrt{\left(\frac{m}{a}\right)^2 + \left(\frac{n}{b}\right)^2}, (m,n) \in \mathrm{Z}^+ \tag{8}$$

Uneven whole numbers in this equation represent the so called "*sloshing frequencies*", while even modes represent "*symmetric frequencies*" as observed in Figure **7**. Generally even modes are induced by symmetric flow features and uneven modes by asymmetric structures (such as jet oscillation)(Gupta *et al.*, 1997).

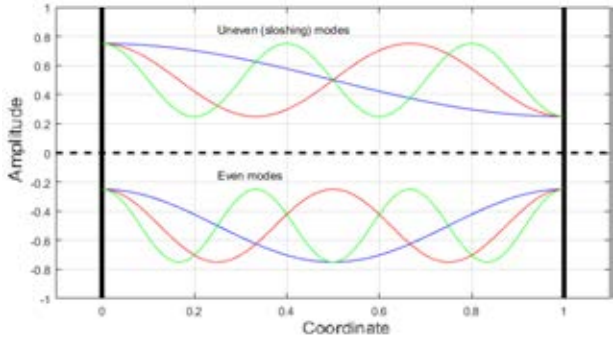


**Figure 7:** Sloshing and symmetric mould frequencies.

These frequencies naturally resonate with the mould and may lead to amplification of the surface waves (i.e. interface fluctuations in the mould); thereby, flow patterns in these frequency ranges must be avoided. Additionally, these frequencies affect the circulation time and roll frequencies. Ultimately the nozzle design affects all these flow structures and plays a major role on how these frequencies are induced.

## RESULTS & VALIDATION

### Overall flow patterns

Processing of CFD results is quite complex since it must portray the long-term behaviour of the flow pattern as well as its frequency fluctuations without simple averaging of the data. Figure 8 presents a volume render of velocities, eddy viscosity and Argon bubbles (i.e. DPM-distribution) for the 1200 x 220 mm mould.

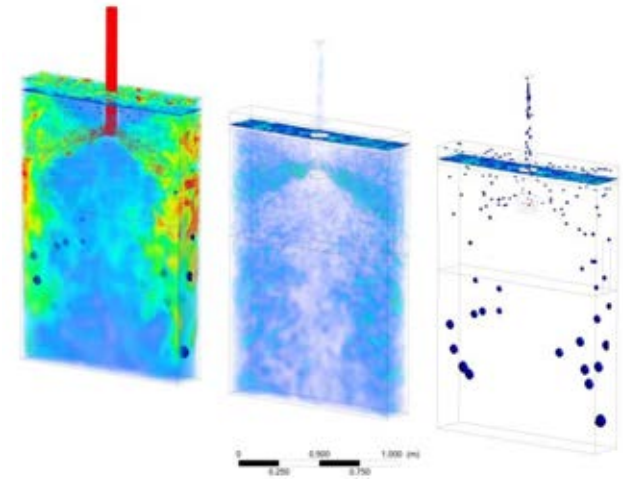

**Figure 8:** Volume render of velocity (left), eddy viscosity (centre) and Argon bubble distribution (right) for a 1200mm×220mm mould with M-type nozzle.

### Steel interface

The steel surface behaviour is of particular interest since the validation depends on the surface behaviour; thus, an iso-surface was used to define the steel-slag interface at VOF=0.5 steel fraction (Figures 9 and 10).

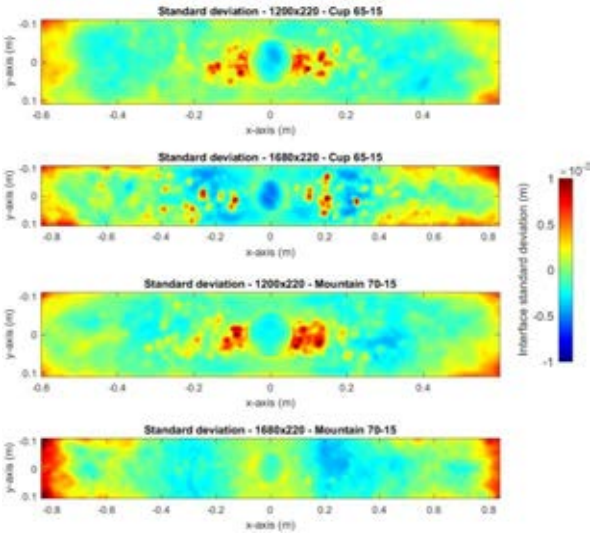


**Figure 9:** Standard Deviation of metal level fluctuations at the free surface.

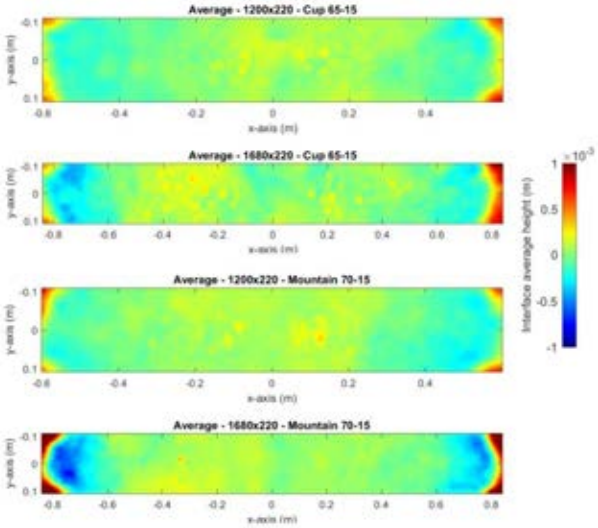


**Figure 10:** Averaging of metal level fluctuations at the free surface (red denotes an increase in level and blue denotes a decrease in level).

The surfaces in Figures 9 and 10 were extracted at a rate of 40 Hz and contain the height of the fluctuations measured from a steady reference level 0.0. (red denotes an increase in level and blue denotes a decrease in level). Figure 9 clearly indicates that the main source of surface fluctuations is the dissipation of momentum at the narrow sides as well as the bubble departure positions. Figure 10 indicates that the most prominent surface feature is the standing wave sending metal upwards due to momentum in the narrow walls and the neighbouring valley (i.e. level depression). This is an interface feature that was confirmed during the plant trials.

### Argon bubbles

The Discrete Phase Model (DPM) is able to predict the argon distribution and flow differences for the various mould sizes. However, there is no method available to map the bubble departure positions during industrial operation and/or liquid metal experiments. Therefore, the results are only indicative of the possible argon behaviour in the mould.

Nevertheless, the flow and velocity patterns observed during plant trials and experiments are similar to those predicted in the CFD simulations. This could well indicate that the argon model predictions are in line with the actual flow patterns in the mould. Bubble departure positions and termination points are presented in Figures 11 and 12, respectively. Figure 11 indicates that the bubble departure positions are spread more evenly for the larger geometry while bubbles tend to cluster around the nozzle for smaller moulds. This is mainly due to the different jet velocities for the widest (1680 mm) and narrowest (1200 mm) moulds. Bubble termination points in the x-y plane (parallel to the wide walls) are shown in Figure 12 where termination points indicate coalescence or escape. Results show that smaller geometries produce more coalescence in the upper part of the nozzle, while bubbles are more evenly distributed for larger geometries. This suggests that the residence times for smaller moulds are significantly larger, which allows more coalescence.

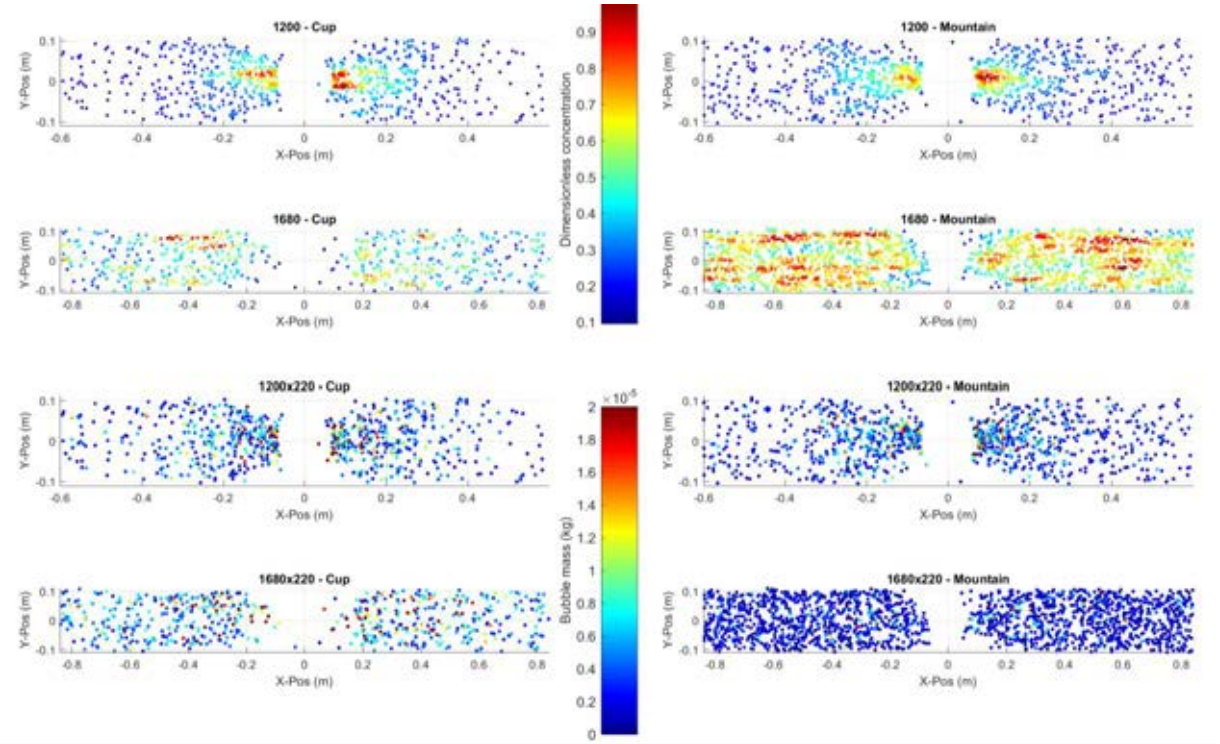


**Figure 11:** Scatter plot of bubble departure positions coloured by dimensionless concentration (upper) and particle mass (lower).

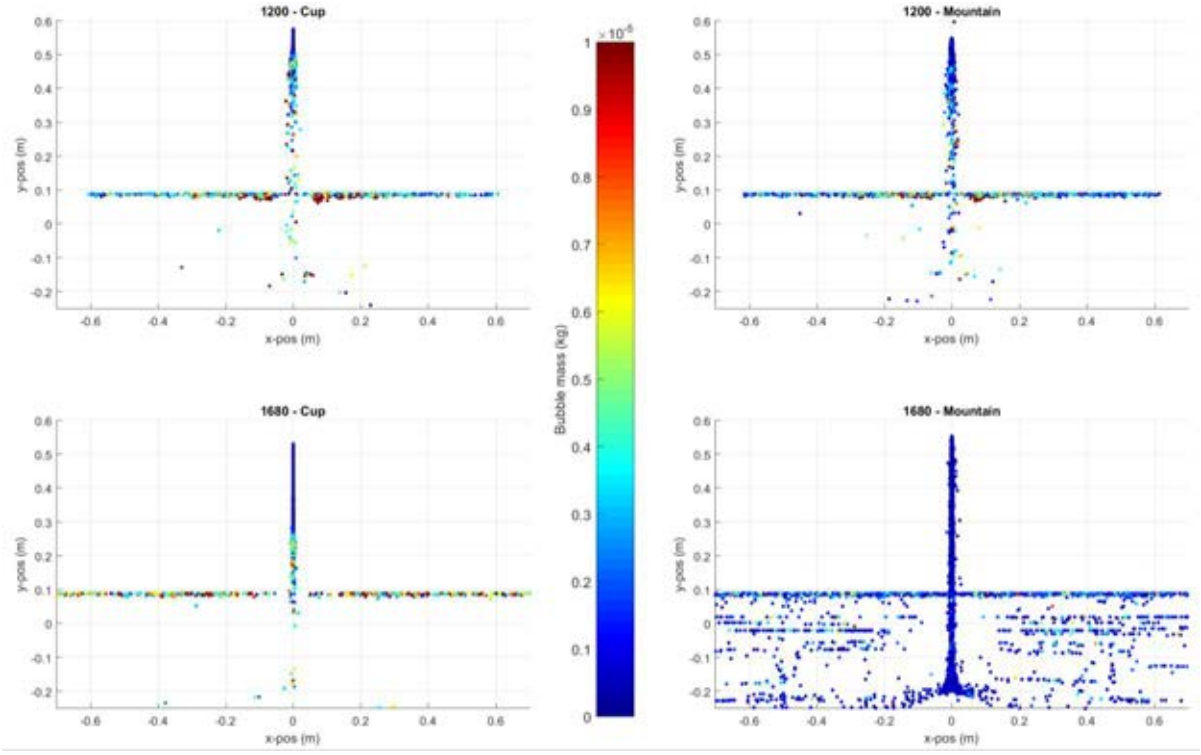


**Figure 12:** Bubbles termination points: y≈0.1 indicates escape while y< or y> 01 indicates coalescence (bubbles coloured by mass at termination).

## Nozzle frequency signature

Predictions show that nozzle performance is the main deciding factor for the length, distribution and periodicity of stable flows within the mould. Furthermore, each particular flow pattern gives rise to a *Nozzle Frequency Signature* (*NFS*) which varies with design, mould geometry and casting speed. Examples of these frequency signatures are presented in Figure 13.

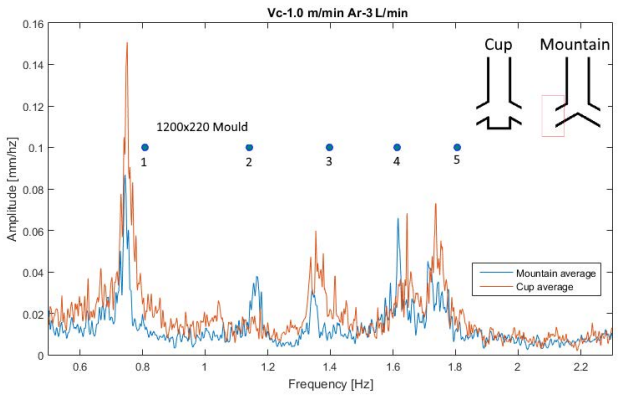


**Figure 13:** NFS for mountain and cup nozzles.

The main nozzle variables which affect NFS for a given mould and casting speed are:

- Inlet angle
- Inlet diameter
- Type (Mountain or Cup)

## Frequency comparison

Table 2 presents the predicted frequencies from analytical and numerical modelling compared to the actual frequencies measured in the physical caster.

**Table 2:** Frequency comparison in Hz

| Peak # | 1 | 2 | 3 | 4 | 5 |
|---|---|---|---|---|---|
| Theoretical | 0.8069 | 1.1412 | 1.3977 | 1.6140 | 1.8045 |
| Numerical | 0.7688 | 1.118 | 1.246 | 1.409 | 1.491 |
| CCS-1.5 | 0.75 | 1.16 | 1.35 | 1.62 | 1.74 |

Results in Table 2 show a good agreement between Theoretical, Numerical and Experimental frequencies, which indicates the validity of the CFD and analytical models developed. Nevertheless, the offsetting of the modelling results towards lower frequencies reveals possible over relaxation as observed in Figure 14. The CFD predictions were further improved by disabling the sharp interface and interfacial anti-diffusion, which provides an excellent match for the Simulator frequencies in Table 3.

**Table 3:** Frequencies from numerical models in Hz (1/s). The number after C or M denotes the port diameter d in mm, while the inlet angle in θ degrees is next. Frequencies in bold numbers have higher amplitudes.

| Peak # | 1 | 2 | 3 | 4 | 5 |
|---|---|---|---|---|---|
| 1200x220 - C 65-15 | **0.778** | x | **1.328** | **1.612** | **1.745** |
| 1200x220 - M 65-15 | **0.709** | 1.211 | **1.471** | 1.588 | 1.720 |
| 1200x220 - M 70-15 | **0.782** | 1.148 | **1.339** | **1.61** | 1.739 |

Substantially better agreement between models and experiments are evident by comparing these frequencies to the physical caster in Table 2. This means that anti-diffusion algorithms should be avoided when modelling mould frequencies and determining the NFS numerically

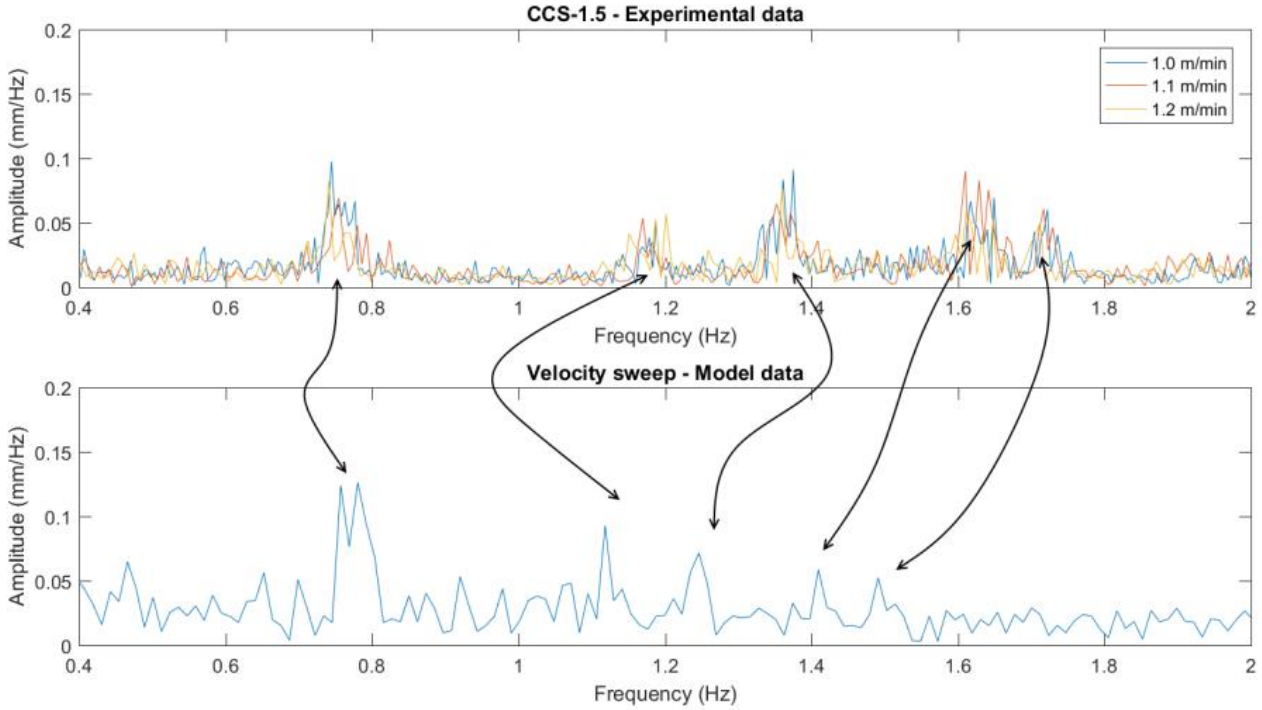


**Figure 14:** Sharp interface numerical model frequencies compared to physical.

### Surface velocity comparison

A comparison between surface velocities in the CFD models and plant measurements is presented in Figures 15 and 16. A dispersed phase formulation is used in Figure 15 for the velocity gradient resulting in poor agreement due to the dispersive layer. In contrast, a sharp anti-diffusive interface formulation is used in Figure 16 resulting in excellent agreement.

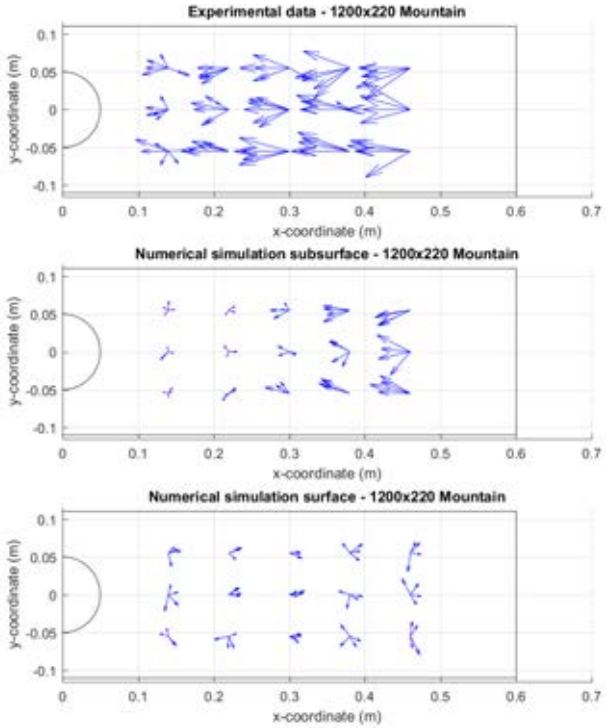


**Figure 15:** Interface velocities for the dispersed phase formulation compared to plant measurements.

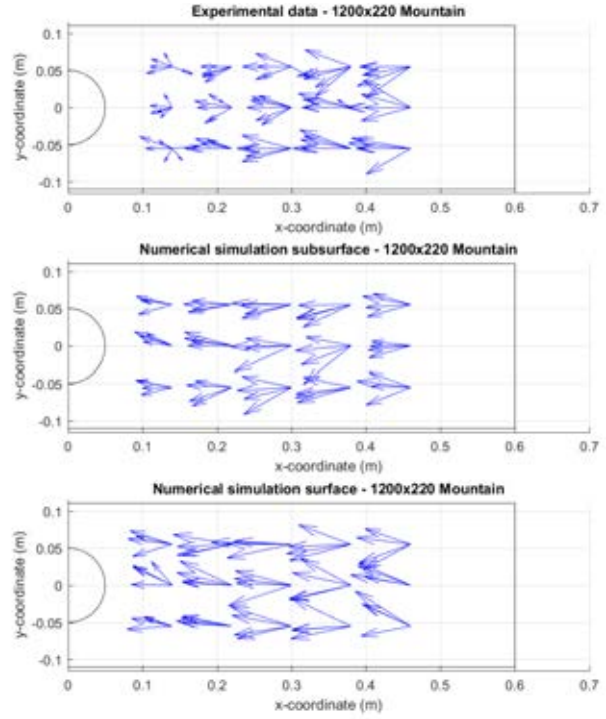


**Figure 16:** Interface velocities for sharp anti-diffusive interface formulation compared to plant measurements.

## DISCUSSION

The combination of LES+VOF+DPM seems suitable to predict the phenomena inside the mould and casting nozzle for different Argon loads and casting speeds. However; at this stage, the model does not account for bubble breakup which is expected to have a minor influence in the flow pattern (i.e. larger bubbles with more buoyancy would have a stronger effect on the flow). The surface velocity comparison shows that a non-dispersive model should be used in order to capture interface velocities with high accuracy. This is the opposite of the surface frequency results in the previous section. This requires further investigations and work is being carried out by the authors to explain and elaborate on these findings.

Ultimately, the aim of the present model is to find optimal conditions for caster operation which includes the ideal bubble size (to avoid entrapment of the bubbles in the solidifying shell). However, this requires coupling of LES with a more complex solidification model as those presented by the authors for a simpler turbulence model; k-epsilon (Ramirez Lopez *et al.*, 2014). This would also imply a non-isothermal solution with the subsequent thermal gradient effects on the continuous and dispersed phases (e.g. gas expansion, increased lift, convective effects, etc.). However, it is expected that these have a minimum impact on the flow since the argon temperature is already close to steel when reaching the injection point as observed by (Iguchi *et al.*, 1995) while the same minor influence can be expected for the convective effects since the inertial forces in the mould are considerably greater than any velocities induced by changes in density of the liquid steel. Even if those become more important towards the end of solidification further down the strand.

## CONCLUSIONS

The present investigation compared results from numerical and analytical models developed for Continuous Casting with Industrial trials and experiments on a Casting Simulator. The following conclusions can be drawn from these comparisons:

- *Eigenfrequencies* in the mould are almost exclusively dependent on the mould geometry, except for offsets in the frequency created by small differences in flow features. These are caused by minor changes in the nozzle design (e.g. port angle and diameter).
- The nozzle performance can be characterized by a Nozzle Frequency Signature (NFS) which varies between mould sizes and casting speed.
- The NFS can be evaluated using numerical methods validated on the Casting Simulator in liquid metal. This allows for a quick and efficient way to test the performance of a nozzle for a given geometry as well as finding optimal casting conditions.
- The analytical approach developed for prediction of frequencies in CC is in very good agreement with experiments and simulations, confirming the existence of the NFS.

- All measurements performed in the CC Simulator clearly show the presence of eigenfrequencies, although the uneven modes are offset compared to the theoretical ones by an average 0.06 Hz.
- It was confirmed that the amplitude of the eigenfrequencies is dependent on nozzle geometry, while the mode amplitudes are dependent on casting speed.
- The dispersed iso-surface VOF model for level monitoring and frequency analysis is proven to better capture the resonance frequencies. However, the sharp interface anti-diffusive interface formulation provides a better agreement with the interface velocities measured industrially.
- The major flow features can be captured using a relatively coarse mesh aiding computational efficiency.

A deeper study is undergoing to study the dependence of the flow patterns on different nozzle parameters such as how the interface, jets and argon-distribution are affected by changes in diameter and inlet angle of the nozzles.

## ACKNOWLEDGEMENTS

The research presented in this paper has been carried out within the project FLOWFLEX- Flow Dynamics studies for Flexible Operation of Continuous Casters (Diarienummer: 2014-01936) funded by the Swedish Innovation Agency, VINNOVA.

## REFERENCES

*ANSYS-INC.: "ANSYS Fluent v.12 - User's Guide", ANSYS Inc., (2013),*

*BARESTRAND, H. and FORSLUND, T.: "Numerical & physical modelling of fluid flow in a continuous casting mould: Flow dynamics studies for flexible operation of continuous casters", (2016),*

*BARESTRAND, H., FORSLUND, T., JALALI, P.N., RAMIREZ LOPEZ, P.E., OLOFSSON, C., ROOS, E. and JÖNSSON, P.: "Flow Dynamics Analysis of Continuous Casting Processes through numerical and Physical Modelling", 4th International Symposium on Cutting Edge of Computer Simulation of Solidification, Casting and Refining (CSSCR2016), (2016), XI'an, CHINA.*

*DAUBY, P.H.: "Real Flows in Continuous Casting Molds", Iron and Steel Technology, **8** (2011), 151-160.*

*GUPTA, D., CHAKRABORTY, S. and LAHIRI, A.K.: "Asymmetry and oscillation of the fluid flow pattern in a continuous casting mould: a water model study", ISIJ International, **37** (1997), 654.*

*IGUCHI, M., CHIHARA, T., TAKANASHI, N., OGAWA, Y., TOKUMITSU, N. and MORITA, Z.-I.: "X-ray fluoroscopic observation of bubble characteristics in a molten iron bath", ISIJ International, **35** (1995), 1354-1361.*

*LIGHTHILL, J.: "Waves in fluids", Cambridge university press, (2001),*

*LIU, R., SENGUPTA, J., CROSBIE, D., CHUNG, S., TRINH, M. and THOMAS, B.G.: "Measurement of molten steel surface velocity with SVC and nail dipping during continuous casting process",TMS Annual Meeting, (2011), 51-58.*

*OLSEN, J.E. and CLOETE, S.W.P.: "COUPLED DPM AND VOF MODEL FOR ANALYSES OF GAS STIRRED LADLES AT HIGHER GAS RATES", Seventh International Conference on CFD in the Minerals and Process Industries, (2009), Melbourne, Australia*

*PERICLEOUS, K., KOUNTOURIOTIS, Z., DJAMBAZOV, G., DOMGIN, J.F. and GARDIN, P.: "Experimental and numerical simulation of the mould region of a steel continuous caster",AIP Conf. Proc., **1281** (2010), 95-98.*

*RAMIREZ LOPEZ, P.E., JALALI NAZEEM, P., SJÖSTRÖM, U. and NILSSON, C.: "Adding Argon Injection through the DPM+VOF Technique to an Advanced Multi-Physics and Multi-Scale Model for Continuous Casting of Steel", 10th International Conference on Computational Fluid Dynamics In the Oil & Gas, Metallurgical and Process Industries, (2014), Trondheim, Norway.*

*RAMIREZ LOPEZ, P.E., JALALI, P.N., BJÖRKVALL, J., SJÖSTRÖM, U. and NILSSON, C.: "Recent developments of a numerical model for continuous casting of steel: Model theory, setup and comparison to physical modelling with liquid metal", ISIJ International, **54** (2014), 342-350.*